Three-Dimensional Dynamic Simulation of Total Knee Replacement Motion During a Step-Up Task

Stephen J. Piazza

Center for Locomotion Studies and Departments of Kinesiology and Mechanical & Nuclear Engineering, Pennsylvania State University, University Park, PA 16802

Scott L. Delp

Biomechanical Engineering Division, Mechanical Engineering Department, Stanford University, Stanford, CA 94305

A three-dimensional, dynamic model of the tibiofemoral and patellofemoral articulations was developed to predict the motions of knee implants during a step-up activity. Patterns of muscle activity, initial joint angles and velocities, and kinematics of the hip and ankle were measured experimentally and used as inputs to the simulation. Prosthetic knee kinematics were determined by integration of dynamic equations of motion subject to forces generated by muscles, ligaments, and contact at both the tibiofemoral and patellofemoral articulations. The modeling of contacts between implants did not rely upon explicit constraint equations; thus, changes in the number of contact points were allowed without modification to the model formulation. The simulation reproduced experimentally measured flexion–extension angle of the knee (within one standard deviation), but translations at the tibiofemoral articulations were larger during the simulated step-up task than those reported for patients with total knee replacements. [DOI: 10.1115/1.1406950]

Introduction

Only a few dynamic knee models (models that use differential equations of motion to relate forces and motions) have been published to date [1,2]. More common have been models in which conditions of static equilibrium have been applied, usually to estimate forces in soft tissues for a series of static configurations (e.g., [3,4]). However, few activities load the knee in the absence of joint motion, and many activities involve large velocities at the knee. Normal walking, for example, is characterized by a rapid knee flexion (greater than 300 deg/s) at toe-off [5]. The application of forces associated with knee injuries are also likely to produce high velocities in the knee joint. Dynamic models, which explicitly link forces and motions, are more appropriate for modeling high-velocity activities than are static models.

Moeinzadeh et al. [6] used a dynamic, planar model of the tibiofemoral joint to quantify ligament and contact loads that resulted from simulated impact forces applied to the tibia. The method of solution used for this model was refined by Engin and Tümer [7]; the authors later added a patella to which a quadriceps force was applied to simulate a kicking motion [8]. Planar models of the tibiofemoral articulation have also been described by Wongchaisuwat et al. [9] and by Abdel-Rahman and Hefzy [10], who later extended their model to three dimensions after improving their solution technique [11]. Patellae have been incorporated into planar dynamic models in which simulated muscle forces drive the motion, including rising from a squat [12] and kicking [13]. However, no three-dimensional dynamic model has yet been described that includes both the tibiofemoral and patellofemoral joints [1].

Existing dynamic knee models have certain elements of their formulation in common: Articular cartilage and the menisci are not considered, bony profiles are described by polynomials or simple shapes, and algebraic equations specifying geometric compatibility conditions at points of articular contact are used to constrain the dynamic equations of motion. A single point of contact is usually assumed to exist at each articulation in planar models.

The three-dimensional model of Abdel-Rahman and Hefzy [11] allowed point contacts at the medial condyle, the lateral condyle, or both condyles; switching from two-point contact to one-point contact involved changing versions of the model. Using such constraint-based techniques to model contact can be troublesome because it requires the development of multiple models to describe all possible sets of constraints and to keep track of the conditions that indicate when models should be switched. Further, it is difficult to model impacts and their associated impulses using constraint forces [7,14].

The purpose of this study was to develop a novel mathematical model of the knee and to incorporate this model into a whole-body, forward-dynamic, musculoskeletal simulation of a step-up task. Two features distinguish this model from previous dynamic knee models: (1) The model is three-dimensional and includes both tibiofemoral and patellofemoral articulations, and (2) the number of contact points at each articulation was permitted to vary throughout the simulation without necessitating a change in the formulation of the contact problem. The present simulation was used to study the motions of total knee replacement components, but the modeling techniques described could also be used to represent the geometry of the natural knee or other joints.

Construction of the Model

Simulated Task. The task involved stepping from the ground up to a 25 cm high step (Fig. 1(A)). Details of the task protocol were specified by Banks et al. [15], who used cinefluoroscopy to quantify *in vivo* implant motions during the step-up task. Step-up was defined to begin just after the left foot breaks contact with the ground and to end just before it makes contact with the top of the step. The simulation was terminated after a predetermined length of time had elapsed equal to the average step duration measured in a normal subject (0.505 s).

Segmental Dynamics. A six-segment model of the human body was developed for use in a forward-dynamic simulation of the step-up task (Figs. 1(B) and 1(C)). The stance (right) leg hip, swing leg hip, and the stance leg ankle were modeled as gimbal joints with three degrees-of-freedom (DOF) each. The foot of the stance leg was fixed to the top step (zero DOF). At the stance leg knee, which contained the prosthesis, the thigh was not con-
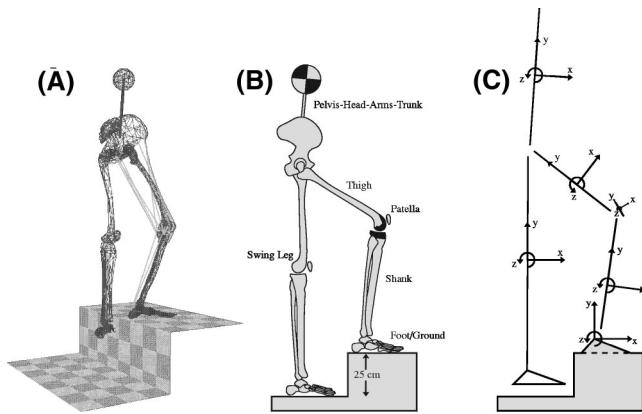
Fig. 1 (**A**) The three-dimensional body model used to simulate step-up. The swing foot passes through the step because knee and ankle motion in the swing leg were not modeled. The stance knee was fitted with a total knee replacement and the stance foot was fixed to the step throughout the simulation. (**B**) Illustration of the six body segments modeled. (**C**) Orientation of each of the six segment-fixed coordinate systems.
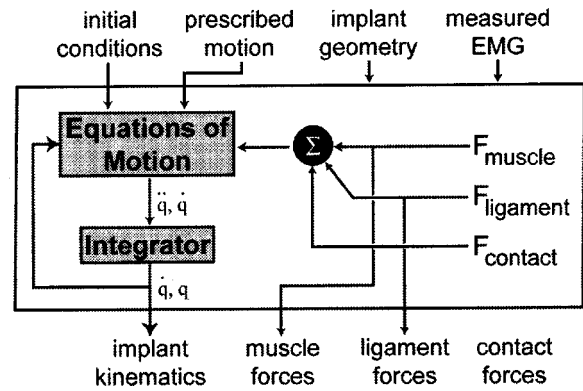

Fig. 2 Flow chart describing the organization of the simulation. Implant motions were determined by using the SD/FAST software package to create differential equations of motion. These equations were numerically integrated to calculate motions while forces were computed and applied that represented the actions of muscles and ligaments and the effects of prescribed motion. SD/FAST input files and routines that computed muscle and ligament forces during the simulation were created using Dynamics Pipeline, a second software package.

strained in its motion relative to the shank (three rotational DOF and three translational DOF); patellofemoral motions were also unconstrained (also six DOF). The model thus had 21 DOF, but the motions of the gimbal joints at the hips and stance ankle were prescribed as functions of time, leaving twelve unprescribed DOF (all at the prosthetic knee; six tibiofemoral DOF and six patellofemoral DOF). The tibiofemoral and patellofemoral motions were not determined by prescribing motion at other joints because, while the relative rotations at the hips and stance ankle were prescribed, the positions of the hips relative to the ground were not prescribed. Inertial parameters were assigned to the segments based on the values derived for a similar model of a 76 kg, 1.8 m tall male by Yamaguchi [16]; Appendix 1 lists these parameter values.

The simulation was implemented on a computer workstation (Silicon Graphics, Inc.; Mountain View, CA) using two software packages: SD/FAST (Symbolic Dynamics, Inc.; Mountain View, CA), which generates symbolic equations of motion and analysis routines using Kane's method [17], and Dynamics Pipeline (MusculoGraphics, Inc.; Evanston, IL), which provides routines for applying muscle forces to the segments and creates SD/FAST input files from existing musculoskeletal models (Fig. 2). These equations are presented in matrix form as

$$\mathbf{M}(q)\dot{q} = \mathbf{V}(q,\dot{q}) + \mathbf{G}(q) + \mathbf{Q_m}(q,\dot{q},a,l_m) + \mathbf{Q_l}(q) + \mathbf{Q_c}(q)$$
$$+ \mathbf{Q_p}(q,\dot{q},t) \tag{1}$$

where

q	=	generalized coordinate vector
$\mathbf{M}(q)$	=	system mass matrix
$\mathbf{V}(q,q)$	=	Coriolis and centripetal effects vector
$\mathbf{G}(q)$	=	gravitational effects vector
$\mathbf{Q_m}(q,\dot{q},a,l_m)$	=	generalized muscle force effects vector
$\mathbf{Q_l}(q)$	=	generalized ligament force effects vector
$\mathbf{Q_c}(q,\dot{q})$	=	generalized articular contact force effects vector
$\mathbf{Q_p}(q,\dot{q},t)$	=	vector of generalized forces used to apply prescribed motions
a	=	muscle activations
l_m	=	muscle fiber lengths

Integration of the equations of motion forward in time during the simulation was accomplished using an SD/FAST routine, which employed a variable time step method based on a fourth-order Runge–Kutta–Merson step.

Musculotendon Modeling. Forces were applied to the segments throughout the simulation to represent the actions of 13 muscles crossing the prosthetic knee. The force-generating capacity of each actuator was characterized by four parameters as proposed by Zajac [18]: optimum fiber length, maximum isometric force, pennation angle, and tendon slack length. Values for these parameters and for the locations of muscle attachment sites, which determined the directions of the muscle forces, were those specified by Delp et al. [19]. Muscle force magnitudes were determined using a Hill-type mathematical model of the musculotendon complex that was originally developed by Schutte et al. [20], who modified the generic Hill-type model described by Zajac [18] by adding a small amount of passive damping to the active contractile element. The equation governing contraction dynamics was of the form

$$\frac{dl_m}{dt} = f_v^{-1}(l_m, l_{mt}, a) \tag{2}$$

where l_{mt} is the total length of the musculotendon actuator, determined from the musculoskeletal geometry, and f_v is the force–velocity relation. Once the time-derivative of the muscle fiber lengths were determined using Eq. (2), values for the muscle fiber lengths were computed by numerical integration. The muscle lengths were used in conjunction with the active and passive muscle force-length curves to determine muscle force [21].

Ligament Modeling. The collateral and patellar ligaments were modeled as purely elastic tensile springs with quadratic force-strain relations of the form

$$F_l = K\varepsilon_l^2 \quad \text{for } l_l \geq l_{lo} \tag{3a}$$

$$F_l = 0 \quad \text{for } l_l < l_{lo} \tag{3b}$$

where F_l is the force produced by the ligament, l_l is the ligament length, K and l_{lo} are a constant of proportionality and a slack length that are specified individually for each ligament fiber, and ε_l is ligament strain [3,22]. A quadratic function was chosen because it was anticipated that collateral ligament strains would be small for the task simulated and the nonlinear toe region would be sufficient to model ligament behavior. The medial and lateral collateral ligaments were represented by two fibers each (anterior and posterior) with attachment sites that produced normal ligament length patterns when normal tibiofemoral motions were pre-

Table 1 Values for the nonlinear ligament stiffness, K, and slack length, l_0. These parameters defined the spring-like properties of the seven ligament fibers modeled (refer to Eqs. (3a) and (3b)). See text for a full description of the sources for these values.

ligament fiber	K (kN)	l_{lo} (mm)
anterior medial collateral	93	74.0
posterior medial collateral	97	80.6
anterior lateral collateral	18	45.2
posterior lateral collateral	18	45.2
medial patellar	58	55.0
central patellar	58	55.0
lateral patellar	58	55.0

scribed [23]. Values of K and l_{lo} for the collateral ligament fibers (Table 1) were computed from estimates of ligament strain in extension derived from experimental measurements made in normal knees by Brantigan and Voshell [24] and Trent et al. [25], as summarized by Wismans et al. [3]. The patellar ligament was represented by three separate fibers (central, medial, and lateral); the attachments of the central fiber on the patella and tibia were those determined by Delp et al. [19]. Medial and lateral patellar ligament attachments were determined by displacing the central fiber attachments by 1 cm medially and laterally. Values of K for these fibers were computed from published experimental data [26] relating tensile stress and strain in a whole patellar ligament. Measurements of the mean width and thickness (3 cm and 3.9 mm, respectively) of the patellar ligament made by Harris et al. [27] were employed to convert the stress–strain relation to the force–strain relation. Values of K for each patellar ligament fiber were derived by dividing the whole-ligament value of K by three. The patellar ligament slack length chosen for all three fibers, 55 mm, was the mean value measured by Bechtold et al. [28] in frozen patellar ligament specimens.

Contact Modeling. Forces representing the effects of contact between the knee replacement components were applied during the simulation. The articulating surfaces of the femoral, tibial, and patellar components were represented by three-dimensional polyhedral meshes consisting of triangles; these meshes were obtained by exporting triangulated geometry from PRO/Engineer (Parametric Technology Corp.; Waltham, MA) representations of the implants. The implants studied were of a commercially available posterior cruciate-substituting design (Osteonics PPSK; Allendale, NJ). Implant surfaces were located with respect to the femur, tibia, and patellar surfaces with the aid of an orthopaedic surgeon who regularly performs knee replacement surgery. Implants were assumed to be rigidly fixed to their respective bones, and were assigned nominal masses and inertial parameters (Appendix 1). The locations of points of implant contact were determined using RAPID, a library of collision detection routines described by Gottschalk et al. [29] that uses hierarchical oriented bounding box representations of surfaces to quickly find triangles in each implant surface that intersect. Locations of edge–face intersections between triangles are then found and assumed to be the contact locations.

Once the locations of points of contact between implants were found, computation of the set of contact forces that prevented implant interpenetration proceeded in the following manner. Im-

plants were considered to be rigid and contact was assumed to occur in the absence of friction. Three conditions were assumed [30]: (1) Implants cannot pull on each other at points of contact, (2) implants cannot accelerate into one another at a point of contact, and (3) either the contact force or the separation acceleration must be zero at each point of contact. When all points of contact are considered simultaneously, these three conditions may be restated as three vector equations:

$$\mathbf{f} \geq \mathbf{0} \tag{4}$$

$$\mathbf{a} = \mathbf{Af} + \mathbf{b} \geq \mathbf{0} \tag{5}$$

$$\mathbf{f}^T \mathbf{a} = \mathbf{f}^T (\mathbf{Af} + \mathbf{b}) = 0 \tag{6}$$

If n points of contact are considered, $\mathbf{f}$, $\mathbf{a}$, and $\mathbf{b}$ are $n \times 1$ vectors containing the magnitudes of the normal contact forces, normal separation accelerations, and normal acceleration components not caused by contact, respectively. $\mathbf{A}$ is an $n \times n$ matrix; A_{ij} represents the normal separation acceleration produced at the ith contact by a unit normal contact force at the jth contact. The components of $\mathbf{A}$ depend on the system masses and mass moments of inertia as well as the locations of the points of contact:

$$A_{ij} = \mathbf{n}_i \cdot \{(1/m)\mathbf{n}_j + [I^{-1}(\mathbf{r}_j \times \mathbf{n}_j)] \times \mathbf{r}_i\}$$

$$\text{when contacts } i,j \text{ involve same body} \tag{7a}$$

$$A_{ij} = 0 \quad \text{otherwise} \tag{7b}$$

where $\mathbf{r}_i$ and $\mathbf{n}_i$ are the vectors specifying the location of the ith contact relative to the segment center of mass and the unit normal to the segment surface at the ith contact, m is the mass of the segment, and I is the inertia tensor of the segment. The problem of solving Eqs. (4)–(6) for $\mathbf{f}$ is known as a linear complementarity problem. This problem was solved during the present simulation using an implementation of Dantzig's algorithm [31] suggested by Baraff [32] to minimize computation time.

If the normal approach velocity at any point of contact exceeded an arbitrarily-determined threshold value (5 mm s^{-1}), an impact was judged to have occurred, the integrator was halted, and the impulses at all points of contact that would arise from the impact were computed. The problem of impulse determination was solved by formulating it as another linear complementarity problem. The separation velocity, $\mathbf{v}^+$, at each point of contact following an impact was assumed to be equal to the approach velocity, $\mathbf{v}^-$, at that contact point multiplied by a coefficient of restitution:

$$\mathbf{v}^+ = -\varepsilon_R \mathbf{v}^- \tag{8}$$

The value for this coefficient (ε_R) is assumed to depend on the material properties, shape, and size of the colliding bodies [33]. A value for ε_R of 0.79, determined from an experiment detailed in Appendix 2, was used for tibiofemoral and patellofemoral collisions. The formulation of the impulse determination problem took the following form [34]:

$$\mathbf{g} \geq \mathbf{0} \tag{9}$$

$$\mathbf{Ag} + (1 + \varepsilon_R)\mathbf{v}^- \geq \mathbf{0} \tag{10}$$

$$\mathbf{g}^T[\mathbf{Ag} + (1 + \varepsilon_R)\mathbf{v}^-] = 0, \tag{11}$$

where $\mathbf{g}$ is the $n \times 1$ vector of normal impulse magnitudes applied at the n contacts, and $\mathbf{A}$ relates impulses to changes in velocity in the same way it related force to acceleration in Eq. (5). The vector of normal impulses, $\mathbf{g}$, was used to compute changes in the velocity and angular velocity at the tibiofemoral and patellofemoral joints, the only non-prescribed joints in the model. Integration of the equations of motion was begun again with the new velocities as the initial conditions.

Experimentally-Derived Kinematic Inputs. Initial conditions and other simulation inputs were derived from experimental

measurements made during the step-ups of a subject with intact knees. These measurements included knee flexion angle and angular velocity at the right knee (the prosthetic knee in the simulation) at the time of toe-off; rotations at the hip and ankle joints that were used to specify prescribed motion at these joints; and measurements of the electromyographic (EMG) activity of seven muscles or groups of muscles crossing the prosthetic knee. All experimental measurements were made using a VICON (Oxford Metrics; Oxford, U.K.) motion analysis system. The subject (29 y.o., 188 cm, 94 kg) was made to step up and down such that each step up/down cycle was approximately 3 s in duration to mimic the step-ups of total knee replacement patients studied by Banks et al. [15]. Data from eleven step-ups were analyzed using MAT-LAB (Mathworks, Inc.; Natick, MA) and VICON Clinical Manager software packages.

The initial tibiofemoral translation was set to correspond to the mean initial locations of the lowest points on the femoral condyles relative to the tibial component reported by Banks et al. [15], approximately 5 mm posterior to the anteroposterior midline of the tibial component at both the medial and lateral condyles. Small changes (1 mm) in the initial anteroposterior tibiofemoral translation did not have a large effect on simulation output. The initial rotation and varus–valgus angles at the prosthetic knee were set to zero to correspond to the observation of Banks et al. [15] that the lowest point on each condyle had nearly the same anteroposterior location. Measurements made in a subject with intact knees were also used to define initial conditions at the replaced knee. The initial knee flexion angle was 52 deg and the knee extension velocity was 120 deg/s; these were the mean values measured at the beginning of step-up. All initial velocities were set to zero at the prosthetic knee with the exception of knee extension velocity. An arbitrary initial position for the patella was chosen and the patella was allowed to oscillate in the presence of transient forces in quadriceps and patellar ligament fibers at the start of a simulation. The simulation was stopped after 5 ms of simulation time and the initial patellofemoral position was adjusted toward the mean of the oscillations. This process was repeated five times prior to a simulation to minimize the amplitude of the initial patellar oscillations.

Motions at the hips and stance ankle of the model were prescribed as functions of time. Each step was normalized to last 0.505 s (the mean duration of the eleven steps; range: 0.405–0.589 s; s.d.: 0.051 s). Fifth-order polynomial functions of time were fit to the mean measured Euler angles; these functions of time and their derivatives were used to prescribe the angles, angular velocities, and angular accelerations of the prescribed joints using routines provided by SD/FAST [35].

Experimentally-Derived Muscle Activation Inputs. Activation inputs to the musculotendon actuators were derived from experimentally measured EMG data and were specified as functions of time. Electrodes were placed on the skin of the subject over seven muscle groups: lateral gastrocnemius, medial gastrocnemius, lateral hamstrings, medial hamstrings, lateral vastus, medial vastus, and rectus femoris. Maximum effort EMG data were collected prior to the step-up trials as the subject performed various static and dynamic tasks. Raw EMG was sampled at 600 Hz and processed by subtracting out the mean voltage and then rectifying. This signal was then digitally filtered in MATLAB, using a fifth-order finite impulse response filter with a low-pass cutoff of 7 Hz. This filtering was performed first in the forward direction and then in the reverse direction to avoid introduction of a phase shift. The filtered data were then normalized in time and averaged over the eleven trials.

Finally, the mean EMG curves were smoothed in MATLAB to obtain activation input curves that both represented the original data and varied smoothly (Fig. 3). Splines were fit to points from these curves and these splines were interpolated to obtain activations during the simulation. The seven activation signals were assigned to the 13 muscles modeled in the following manner:
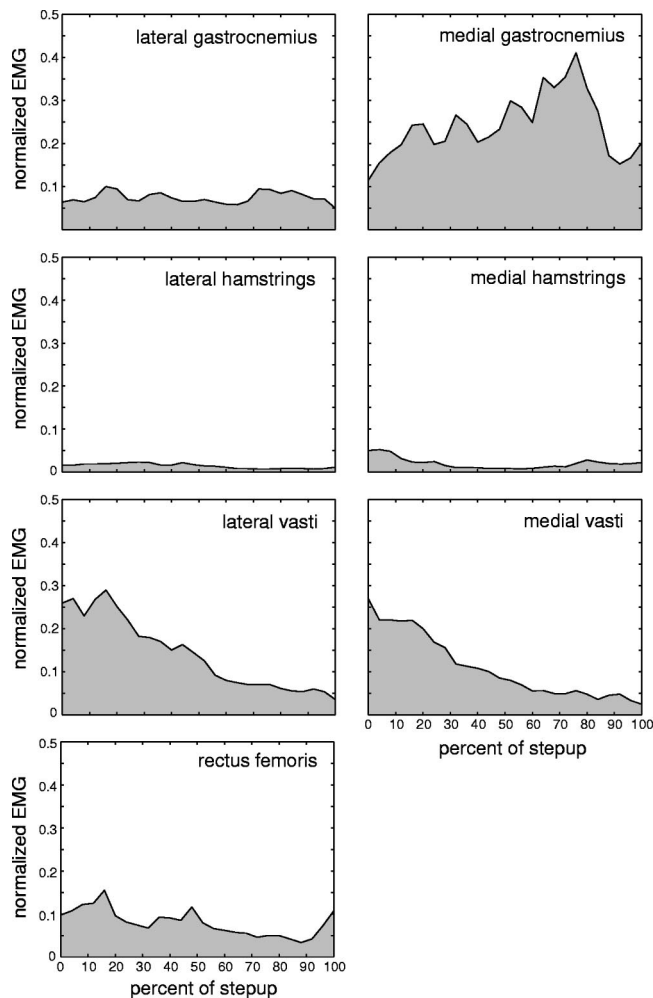

Fig. 3 EMG data that has been rectified, filtered, averaged, and smoothed. These seven curves were used to prescribe the activation input of 11 of the 13 musculotendon actuators. The two remaining actuators, representing tensor fascia lata and sartorius, received no activation input.

semimembranosus, semitendinosus and gracilis received medial hamstrings EMG; biceps femoris long head and short head received lateral hamstrings EMG; vastus intermedius received the EMG measured in vastus lateralis. The medial and lateral gastrocnemius, medial and lateral vasti, and rectus femoris received inputs from their corresponding measured EMG. Two muscles, tensor fascia lata and sartorius, received no activation input but could develop passive force in response to stretch during the simulation.

Results

Knee flexion angles computed during the simulated step-up compared favorably to those measured in a normal subject and to observations made during the step-ups of patients with total knee replacements. The simulated knee flexion versus time trajectory was within one standard deviation of the measured knee flexion mean derived by averaging over 11 trials (Fig. 4). The simulated femur rotated externally with respect to the tibia from zero to 7.5 deg during step-up, close to the value for rotational range of motion reported by Banks et al. [15] (4.9 ± 2.4 deg).

The net intersegmental forces at the knee in the simulation were smaller than the average values computed from measurements made by Banks et al. [36] of the step-ups of five knee replacement patients using inverse-dynamic analysis (Fig. 5). These forces were computed for the model from simulated ground reaction
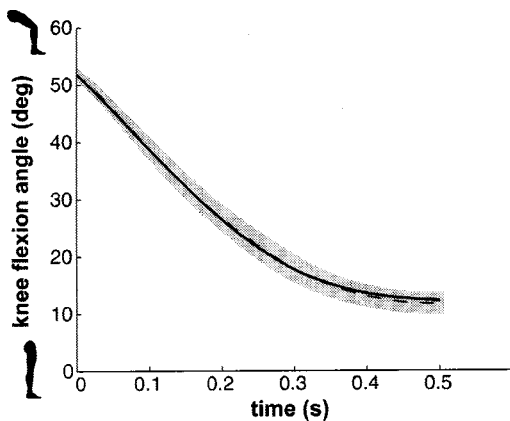
Fig. 4 Knee flexion versus time during step-ups performed by a normal subject (dashed line and shaded area represent the mean and one standard deviation above and below the mean), and simulated knee flexion (solid line)

forces and segment accelerations. Simulated anterior–posterior and medial–lateral net knee forces compared favorably with those of knee replacement patients, but net forces in the superior–inferior direction in the simulation were approximately 50 percent of experimentally measured values. Resultant contact forces at the tibiofemoral articulation were also calculated for the simulation (Fig. 5); such forces cannot be compared to forces measured *in vivo* unless patients have been fitted with instrumented prostheses.

Simulated tibiofemoral translations were slightly different from those measured in knee replacement patients using cinefluoroscopy (Fig. 6). Five patients studied by Banks et al. [15] performed a step-up task identical to that specified in the simulation and had knee replacements of the same posterior cruciate-substituting design as those modeled in the present study. The measured antero-posterior position of the lowest points on the femoral component relative to the tibial component remained nearly constant as the knee extended. In the simulation, however, these points initially moved forward by approximately 5 mm before reversing direction when the knee reached about 30 deg flexion. The magnitude of the separation between the femoral cam and tibial spine that occurred during simulated step-up was similar to that measured in three patients by Banks et al. [15], but this separation began later in the motion (at a knee flexion angle of 30 deg rather than 40 deg) in the simulation.

The ratio of patellar ligament force to force in the quadriceps tendon in the model approximated measurements reported in previous studies of natural cadaver knees (Fig. 7). Values for this ratio are an important simulation output because the extensor mechanism of the knee is the only source of active knee extension moment; the resulting knee extension is the motion that chiefly characterizes step-up. The sum of all quadriceps forces reached a peak of 1150 N (1.54 body weights) at the outset of the simulation. Collateral ligament forces were negligible throughout the simulation, with only the anterior fibers of MCL generating small forces of less than 5 N.

Discussion

The simulation described in this paper is the first dynamic knee model to allow three-dimensional motion at both the tibiofemoral and patellofemoral articulations subject to forces produced by muscles, ligaments, articular contact, and passive dynamics. The use of a forward-dynamic formulation is appropriate and necessary for this purpose because it involves the application of forces to produce motions rather than the computation of forces for a given motion performed in inverse dynamics. In addition, the simulated knee has been placed into a whole-body model as it performs a task that is clinically relevant to total knee replacement
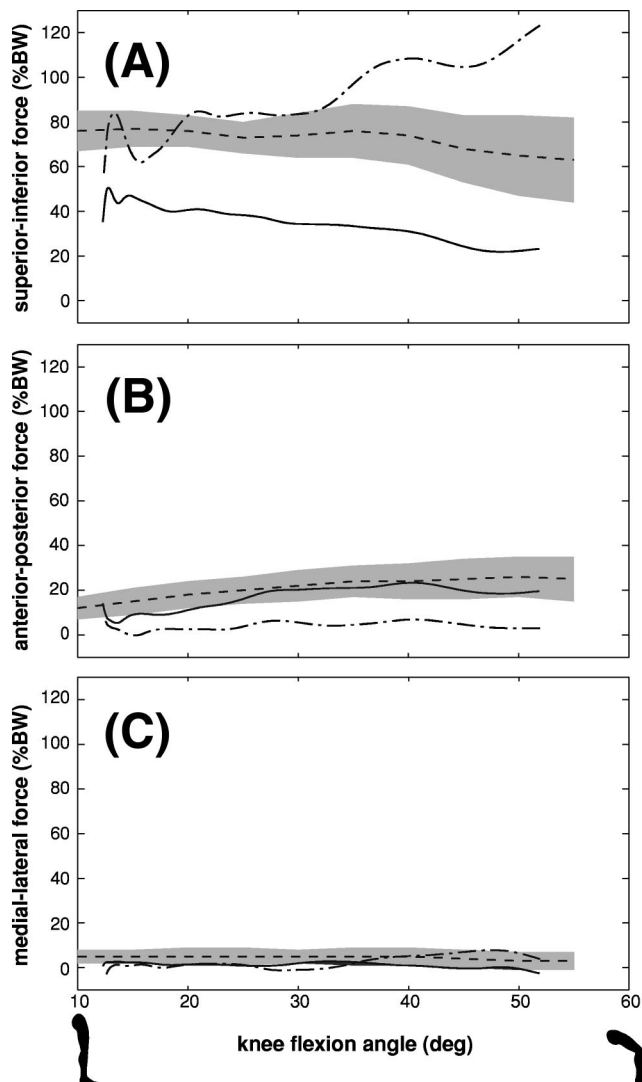

Fig. 5 Simulated and measured forces at the prosthetic knee plotted against knee flexion angle. Net intersegmental forces at the knee in the present simulation (solid curves) were defined as the difference between resultant muscle force and the articular contact force [44]. Corresponding net intersegmental forces, averaged over five patients with posterior cruciate-substituting knee implants, were reported by Banks et al. [36] (dashed curves with shading representing ± one standard deviation). All forces have been normalized by body weight (BW). The components of the tibiofemoral articular contact forces (dash-dot curves) are also presented. (A) Superior–inferior forces. Positive net force indicates a net upward force applied to the tibia and positive articular contact force indicates a force applied to the tibia downward along its long axis. (B) Anterior–posterior forces. Positive net force is in the anterior direction and positive articular contact force indicates a posteriorly directed force applied to the tibia. (C) Medial–lateral forces. Positive net force is in the lateral direction and positive articular contact force indicates a medially directed force applied to the tibia.

patients. This type of simulation permits the study of the behavior of an artificial knee in a simulated *in vivo* environment. Certain aspects of the simulation output, such as knee joint angle (Fig. 4) and the ratio of patellar ligament forces to quadriceps forces (Fig. 7), showed good agreement with experimental measurements but others did not. The limitations of the model that are likely to be responsible for discrepancies between simulation and experiment are discussed below.

Fig. 7 Ratios of patellar ligament force (F_{pl}) to quadriceps force (F_q) computed during the present simulation and measured in cadavers [45–47].
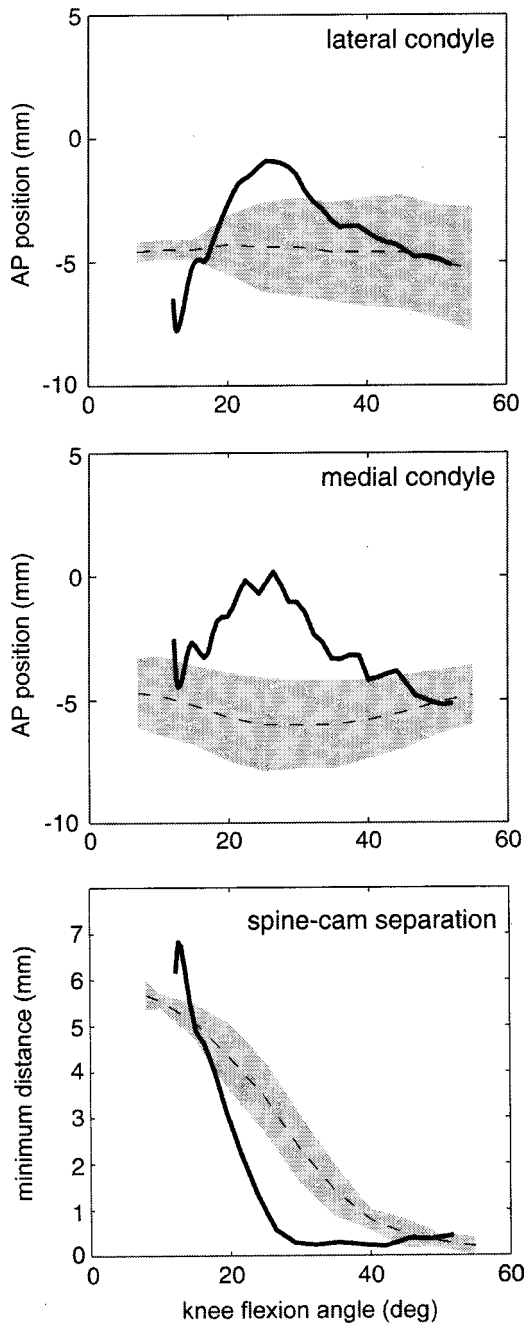
Fig. 6 Anteroposterior positions of the lowest points on the lateral (*top*) and medial (*middle*) femoral condyles relative to the tibial component, and the minimum distance separating the femoral cam and tibial spine (*bottom*). Anteroposterior condyle positions are specified relative to the anteroposterior midline of the tibial component (anterior positive). Dashed lines with shading are the mean lowest-point positions (±one standard deviation) and spine-cam separations measured by Banks et al. [15] in patients who had received the same implant as that modeled in the present study.

The limitations of the model must be evaluated and addressed before it is used to study problems of clinical interest. Tibiofemoral translations were smaller in patients than in the simulation (Fig. 6), suggesting that the model may be underconstrained. There are several possible causes of insufficient constraint, including diminished axial compressive forces at the knee. The net intersegmental forces at the knee in the simulation were only half of what Banks et al. [36] measured in patients performing an identi-
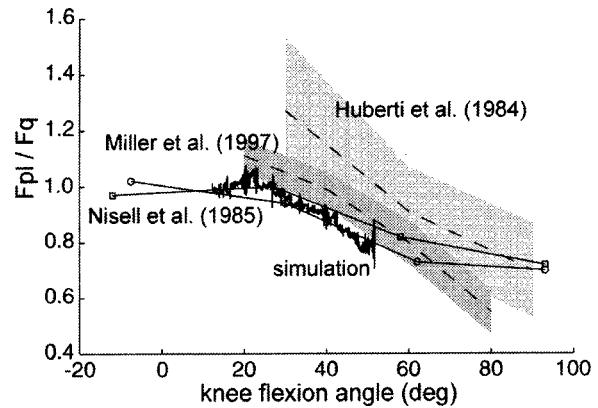
cal step-up task (Fig. 5), and the tibiofemoral contact forces in the simulation were only about half of those measured during stair ascent using an instrumented prosthesis by Taylor et al. [37]. These smaller-than-expected net and contact forces may signify that the axial compressive forces produced by muscles are unrealistically small as well. The assumption that articular contact was frictionless is also likely to have contributed to lack of constraint; Sathasivam and Walker [38] reported large differences in implant kinematics caused by changes in coefficient of friction using a static computer model of total knee replacement.

Underestimation of the net intersegmental knee force in the simulation was likely to have been caused by the simulated ground reaction force, from which net force was calculated, being too small. This insufficiency in the simulated ground reaction force was probably caused by accelerations of massive body segments being slightly different from those of their real counterparts, resulting in unrealistic accelerations of the whole-body center of mass. Further simulations were performed in which small variations were made in the motion prescribed for the hips and stance ankle; it was found that ground reaction forces could be increased in this way. Levels of net intersegmental knee force seen in patients, however, could not be attained by varying the prescribed motion, and we attribute this failure to a lack of the necessary degrees of freedom. Proper motion of the center of mass is difficult to achieve without joints between the pelvis and trunk, or between the head and neck. A more complicated model that includes these joints has greater potential to reproduce realistic ground reaction forces. Underestimation of ground reaction force by simulations has been reported previously [39,40], and Stauffer et al. [41] demonstrated that subjects with similar joint motions may exhibit ground reaction forces that are very different.

The contact modeling used in the present simulation has benefits and limitations. Unlike those described previously, the present knee model does not rely on explicit constraints specifying the nature or number of contacts between implants. Contact forces are computed as the solution of a linear complementarity problem rather than by solution of a less tractable system of differential algebraic equations. The contact model is limited, however, by the assumption that the implants are rigid bodies. If deformation of the implants is not allowed and there are multiple points of contact, as in the present simulation, solving for the contact forces becomes an indeterminate problem. The result of this indeterminacy is that the set of contact forces in **f** (Eqs. (4–6)) is generally not unique. The set of accelerations in **a**, however, is unique; a proof of this result was published by Cottle [42]. The uniqueness of the accelerations and non-uniqueness of the contact forces may mean that this contact model is appropriate for understanding implant motions but ill-suited for quantifying contact forces. This limitation could be addressed by implementing a con-

tact force determination scheme in which the repulsive force at each point of contact depends on the degree of penetration, material properties, and surface geometry.

Many of the limitations of the model discussed above could be addressed by driving the simulation with a set of input data derived solely from patients with total knee replacements; unfortunately, such data are not presently available. Such a data set would also provide greater potential for validation of the simulation output. Changing the formulation of the model to incorporate an optimization algorithm [43] to determine muscle excitation inputs that permit the model to track measured kinematic or kinetic variables (such as knee flexion angle and ground reaction force) would also likely result in a more realistic simulation. How implant motions are affected by changes in implant geometry, surgical placement of the components, ligament releases, and muscle weakness are all areas of clinical interest that may be addressed using a future version of the present model that incorporates these improvements.

Acknowledgments

Appendix 1

The inertial parameters for the model segments were those specified by Yamaguchi [16]. Values for the segment masses and mass moments of inertia are given in Table 2. Values defining the center of mass locations relative to the joints are specified in Table 3.

Appendix 2

Newton's Law of Restitution states that when two bodies collide, the separation velocity (ν^+) is related to the approach velocity (ν^-) by a constant of proportionality called the coefficient of restitution [33]:

$$\nu^+ = -\varepsilon_R \nu^-. \tag{12}$$

This coefficient may be assumed to depend on the material properties of the colliding bodies and their geometry near the point of

Table 3 Components of vectors defining locations of joints relative to segment centers of mass. Each vector a $=\langle a_x, a_y, a_z \rangle$ points from a segment center of mass to a joint that connects that segment to a neighboring segment, where these components of a are aligned with the coordinate systems attached to the center of mass of each segment and oriented as shown in Fig. 1(C). All values for body segment inertial parameters are derived from Yamaguchi [16].

center of mass	joint	a_x (m)	a_y (m)	a_z (m)
pelvis-head-arms-trunk	stance hip	-0.084	-0.427	0.084
pelvis-head-arms-trunk	swing hip	-0.084	-0.427	-0.084
stance thigh	stance hip	0.0	0.183	0.0
stance shank	stance ankle	0.0	-0.247	0.0
swing leg	swing hip	-0.004	0.367	0.0

contact. Other factors, such as temperature and the magnitude of the approach velocity, may also affect this relationship.

A simple experiment was performed to determine the coefficient of restitution for impacts between knee replacement components. Collisions between a solid chrome-steel ball with a diameter of 1 in. (meant to represent a condyle of a Co–Cr femoral component) and a 12 in.$\times$12 in.$\times$3/8 in. sheet of ultra-high molecular weight polyethylene (meant to represent the tibial insert of a tibial component) were studied. Velocities just prior to and just following an impact are difficult to measure directly; instead, the ball was dropped from a known height, h^-, onto the sheet and the height of its rebound, h^+, was recorded. Neglecting air resistance, it was possible to compute ε_R from the initial and final heights using conservation of energy:

$$mgh^- = 0.5m(\nu^-)^2 \tag{13}$$

$$mgh^+ = 0.5m(\nu^+)^2 \tag{14}$$

$$\varepsilon_R = \nu^+/\nu^- = (h^+/h^-)^{0.5} \tag{15}$$

The polyethylene sheet was rigidly clamped to a steel fixture, which was bolted to the structural supports of the laboratory. Steel balls were dropped inside a Plexiglas tube (1.25 in. I.D.) to which a ruler was affixed, and measurement of the initial and final heights were accomplished using a video camera recording with a shutter speed of 1/60 s. Thirty trials were performed from varied initial heights; ten drops each were carried out from approximately 2, 4, and 6 cm. Videotape of the ball drops was analyzed using a videocassette player with frame-by-frame capability.

The square root of the final height was plotted versus the square root of the initial height for each ball drop. A highly linear relationship ($R^2 = 0.99$) was found and the slope of the regression line, 0.79, was taken to be the coefficient of restitution.

Table 2 Masses and mass moments of inertia for the body segments. All moments of inertia are principle moments of inertia (products of inertia are zero) except for those of the pelvis-head-arms-trunk segment. The pelvis-head-arms-trunk was modeled with arms outstretched in front of the trunk; the asymmetry of this configuration resulted in a nonzero $I_{xy}(-0.472 \text{ kg m}^2)$. Nominal inertial parameters were used for the patella and for the knee replacement components. All values for body segment inertial parameters were derived from Yamaguchi [16].

segment	mass (kg)	I_{xx} (kg m^2)	I_{yy} (kg m^2)	I_{zz} (kg m^2)
pelvis-head-arms-trunk	51.22	1.980	2.978	4.084
stance thigh	7.58	0.126	0.080	0.126
stance shank	3.75	0.065	0.019	0.065
swing leg	12.43	0.943	0.110	0.952
stance patella	0.025	2e-6	2e-6	2e-6
femoral component	0.1	4e-5	4e-5	4e-5
tibial component	0.1	4e-5	4e-5	4e-5
patellar component	0.025	2e-6	2e-6	2e-6

References

[1] Hefzy, M. S., and Cooke, T. D. V., 1996, "Review of Knee Models: 1996 Update," Appl. Mech. Rev., **49**, pp. S187–S193.
[2] Hefzy, M. S., and Grood, E. S., 1988, "Review of Knee Models," Appl. Mech. Rev., **41**, pp. 1–13.
[3] Wismans, J., Veldpaus, F., Janssen, J., Huson, A., and Struben, P., 1980, "A Three-Dimensional Mathematical Model of the Knee-Joint," J. Biomech., **13**, pp. 677–685.
[4] Yamaguchi, G. T., and Zajac, F. E., 1989, "A Planar Model of the Knee Joint to Characterize the Knee Extensor Mechanism," J. Biomech., **22**, pp. 1–10.
[5] Piazza, S. J., and Delp, S. L., 1996, "The Influence of Muscles on Knee Flexion During the Swing Phase of Gait," J. Biomech., **29**, pp. 723–733.
[6] Moeinzadeh, M. H., Engin, A. E., and Akkas, N., 1983, "Two-Dimensional

Dynamic Modelling of Human Knee Joint," J. Biomech., **16**, pp. 253–264.

[7] Engin, A. E., and Tümer, S. T., 1993, "Improved Dynamic Model of the Human Knee Joint and Its Response to Impact Loading on the Lower Leg," ASME J. Biomech. Eng., **115**, pp. 137–143.

[8] Tümer, S. T., and Engin, A. E., 1993, "Three-Body Segment Dynamic Model of the Human Knee," ASME J. Biomech. Eng., **115**, pp. 350–356.

[9] Wongchaisuwat, C., Hemami, H., and Buchner, H. J., 1984, "Control of Sliding and Rolling at Natural Joints," ASME J. Biomech. Eng., **106**, pp. 368–375.

[10] Abdel-Rahman, E., and Hefzy, M. S., 1993, "A Two-Dimensional Dynamic Anatomical Model of the Human Knee Joint," ASME J. Biomech. Eng., **115**, pp. 357–365.

[11] Abdel-Rahman, E. M., and Hefzy, M. S., 1998, "Three-Dimensional Dynamic Behaviour of the Human Knee Joint Under Impact Loading," Med. Eng. Phys., **20**, pp. 276–290.

[12] Kim, S., and Pandy, M. G., 1993, "A Two-Dimensional Dynamic Model of the Human Knee Joint," Biomed. Sci. Instrum., **29**, pp. 33–46.

[13] Tümer, S. T., Wang, X., and Akkas, N., 1995, "A Planar Dynamic Anatomical Model of the Human Lower Limb," Biomed. Eng.—Applications, Basis & Communications, **7**, pp. 365–378.

[14] Mirtich, B., and Canny, J., 1995, "Impulse-Based Simulation of Rigid Bodies," *Proc. 1995 Symposium on Interactive 3D Graphics*, pp. 181–188.

[15] Banks, S. A., Markovich, G. D., and Hodge, W. A., 1997, "In Vivo Kinematics of Cruciate-Retaining and -Substituting Knee Arthroplasties," J. Arthroplasty, **12**, pp. 297–304.

[16] Yamaguchi, G. T., 1989, "Feasibility and Conceptual Design of Functional Neuromuscular Stimulation Systems for the Restoration of Natural Gait to Paraplegics Based on Dynamic Musculoskeletal Models," Ph.D. Dissertation, Stanford University, Stanford, CA.

[17] Rosenthal, D. E., and Sherman, M. A., 1986, "High Performance Multibody Simulations via Symbolic Equation Manipulation and Kane's Method," J. Astronaut. Sci., **34**, pp. 223–239.

[18] Zajac, F. E., 1989, "Muscle and Tendon: Properties, Models, Scaling, and Application to Biomechanics and Motor Control," Crit. Rev. Biomed. Eng., **17**, pp. 359–411.

[19] Delp, S. L., Loan, J. P., Hoy, M. G., Zajac, F. E., Topp, E. L., and Rosen, J. M., 1990, "An Interactive Graphics-Based Model of the Lower Extremity to Study Orthopaedic Surgical Procedures," IEEE Trans. Biomed. Eng., **37**, pp. 757–767.

[20] Schutte, L. M., Rodgers, M. M., Zajac, F. E., and Glaser, R. M., 1993, "Improving the Efficacy of Electrical Stimulation-Induced Leg Cycle Ergometry: An Analysis Based on a Dynamic Musculoskeletal Model," IEEE Trans. Rehabil. Eng., **1**, pp. 109–125.

[21] Delp, S. L., and Loan, J. P., 1995, "A Graphics-Based Software System to Develop and Analyze Models of Musculoskeletal Structures," Comput. Biol. Med., **25**, pp. 21–34.

[22] Mommersteeg, T. J., Blankevoort, L., Huiskes, R., Kooloos, J. G., and Krauer, J. M., 1996, "Characterization of the Mechanical Behavior of Human Knee Ligaments: A Numerical–Experimental Approach," J. Biomech., **29**, pp. 151–160.

[23] Piazza, S. J., Delp, S. L., Stulberg, S. D., and Stern, S. H., 1998, "Anterior Placement of the Femoral Component in Total Knee Replacement Produces Collateral Ligament Laxity," Trans. 44th Annu. Meet. — Orthop. Res. Soc., p. 1028.

[24] Brantigan, O. C., and Voshell, A. F., 1941, "The Mechanics of the Ligaments and Menisci of the Knee Joint," J. Bone Jt. Surg., Am. Vol., **23**, pp. 44–66.

[25] Trent, P. S., Walker, P. S., and Wolf, B., 1976, "Ligament Length Patterns, Strength, and Rotational Axes of the Knee Joint," Clin. Orthop. Relat. Res., **117**, 263–70.

[26] Haut, R. C., and Powlison, A. C., 1990, "The Effects of Test Environment and Cyclic Stretching on the Failure Properties of Human Patellar Tendons," J. Orthop. Res., **8**, pp. 532–540.

[27] Harris, N. L., Smith, D. A., Lamoreaux, L., and Purnell, M., 1997, "Central Quadriceps Tendon for Anterior Cruciate Ligament Reconstruction. Part I: Morphometric and Biomechanical Evaluation," Am. J. Sports Med., **25**, pp. 23–28.

[28] Bechtold, J. E., Eastlund, D. T., Butts, M. K., Lagerborg, D. F., and Kyle, R. F., 1994, "The Effects of Freeze-Drying and Ethylene Oxide Sterilization on the Mechanical Properties of Human Patellar Tendon," Am. J. Sports Med., **22**, pp. 562–566.

[29] Gottschalk, S., Lin, M. C., and Manocha, D., 1996, "OBBTree: A Hierarchical Structure for Rapid Interference Detection," *Proc. ACM SIGGRAPH Conference on Computer Graphics*, pp. 171–180.

[30] Lötstedt, P., 1982, "Mechanical Systems of Rigid Bodies Subject to Unilateral Constraints," SIAM (Soc. Ind. Appl. Math.) J. Appl. Math., **42**, pp. 281–296.

[31] Cottle, R. W., and Dantzig, G. B., 1968, "Complementary Pivot Theory of Mathematical Programming," *Linear Algebra and Its Applications*, Vol. 1, pp. 103–125.

[32] Baraff, D., 1994, "Fast Contact Force Computation for Nonpenetrating Rigid Bodies," *Proc. ACM SIGGRAPH Conference on Computer Graphics*, pp. 23–34.

[33] Beer, F. P., and Johnston, E. R., 1988, *Vector Mechanics for Engineers: Statics and Dynamics*, McGraw-Hill, New York.

[34] Baraff, D., 1989, "Analytical Methods for Dynamic Simulation of Nonpenetrating Rigid Bodies," *Trans. ACM Siggraph*, pp. 223–232.

[35] Piazza, S. J., 1998, "Simulation-Based Design of Total Knee Replacements," Ph.D. Dissertation, Northwestern University, Evanston, IL.

[36] Banks, S. A., Backus, S. I., Otis, J. C., Haas, S. B., and Laskin, R. S., 2000, "Motions and Forces in Total Knee Replacements During Stair Rise," Trans. 46th Annu. Meet. — Orthop. Res. Soc., p. 431.

[37] Taylor, S. J., Walker, P. S., Perry, J. S., Cannon, S. R., and Woledge, R., 1998, "The Forces in the Distal Femur and the Knee During Walking and Other Activities Measured by Telemetry," J. Arthroplasty, **13**, pp. 428–437.

[38] Sathasivam, S., and Walker, P. S., 1997, "A Computer Model With Surface Friction for the Prediction of Total Knee Kinematics," J. Biomech., **30**, pp. 177–184.

[39] Mochon, S., and McMahon, T. A., 1980, "Ballistic Walking: An Improved Model," Math. Biosci., **52**, pp. 241–260.

[40] Yamaguchi, G. T., and Zajac, F. E., 1990, "Restoring Unassisted Natural Gait to Paraplegics via Functional Neuromuscular Stimulation: A Computer Simulation Study," IEEE Trans. Biomed. Eng., **37**, pp. 886–902.

[41] Stauffer, R. N., Chao, E. Y., and Brewster, R. C., 1977, "Force and Motion Analysis of the Normal, Diseased, and Prosthetic Ankle Joint," Clin. Orthop. Relat. Res., **127**, pp. 189–196.

[42] Cottle, R. W., 1968, "On a Problem in Linear Equalities," J. London Math. Soc., **43**, pp. 378–384.

[43] Neptune, R. R., and Hull, M. L., 1998, "Evaluation of Performance Criteria for Simulation of Submaximal Steady-State Cycling Using a Forward Dynamic Model," ASME J. Biomech. Eng., **120**, pp. 334–341.

[44] Winter, D. A., 1979, *Biomechanics of Human Movement*, Wiley, New York.

[45] Huberti, H. H., Hayes, W. C., Stone, J. L., and Shybut, G. T., 1984, "Force Ratios in the Quadriceps Tendon and Ligamentum Patellae," J. Orthop. Res., **2**, pp. 49–54.

[46] Miller, R. K., Murray, D. W., Gill, H. S., O'Connor, J. J., and Goodfellow, J. W., 1997, "In Vitro Patellofemoral Joint Force Determined by a Non-Invasive Technique," Clin. Biomech., **12**, pp. 1–7.

[47] Nisell, R., 1985, "Mechanics of the Knee. A Study of Joint and Muscle Load With Clinical Applications," Acta Orthop. Scand. Suppl., **216**, pp. 1–42.